The multiple atomic configuration and formation mechanisms of extended defects in wurtzite GaN

2000 J. Phys.: Condens. Matter 12 10185

(http://iopscience.iop.org/0953-8984/12/49/318)

J. Phys.: Condens. Matter **12** (2000) 10185–10194. Printed in the UK PII: S0953-8984(00)17519-8

The multiple atomic configuration and formation mechanisms of extended defects in wurtzite GaN

P Ruterana†, J Chen, V Potin and G Nouet

ESCTM-CRISMAT, Institut des Sciences de la Matière et du Rayonnement, 6 Boulevard Maréchal Juin, 14050 Caen Cedex, France

E-mail: ruterana@lermat8.ismra.fr

Received 28 September 2000

Abstract. In this work, extensive experimental investigation has been carried out by high resolution electron microscopy on most of the known extended defects (threading dislocations, inversion domain boundaries and stacking faults).

The threading dislocations have their lines mainly parallel to the growth axis and more than 90% are of $\boldsymbol{a}$ type. It was then possible to analyse their atomic structure by observing them along the [0001] zone axis. It was found that in the best layers, where their density is below 10^{10} cm^{-2}, the threading dislocations bear two atomic configurations with eight atom cycles or 5/7 rings along their line. In highly defective layers, large angle boundaries have been observed and an additional four atom ring core has been found.

When inversion domains are present, they are bounded by $\{10\bar{1}0\}$ facets and their boundaries were found either to exhibit Ga–Ga and N–N bonds or to be reconstructed. The two atomic configurations are related by a $c/2$ translation. Although $\{10\bar{1}0\}$ non-inversion boundaries have been reported in GaN layers, in our samples, the only non-inversion boundaries we have found lie in $\{11\bar{2}0\}$ lattice planes. A thorough investigation has shown that they are prismatic faults and two atomic configurations have been observed: they have $1/2\langle 10\bar{1}1\rangle$ and $1/6\langle 20\bar{2}3\rangle$ displacement vectors respectively.

The $\{11\bar{2}0\}$ stacking faults have been found to easily fold from the prismatic to the basal planes and to originate from a surface step in the case of growth on (0001) SiC. The formation of inversion domains has been shown to minimize the misfit along the c axis in the case of the nanometric step network at the (0001) sapphire surface.

1. Introduction

III–V nitrides are good candidates for optoelectronic applications from red to ultra-violet. However the fabrication of devices has encountered intrinsic problems due to the lack of bulk substrates which has motivated a world wide research effort. Light emitting diodes were available from 1993 and laser emission was demonstrated at the end of 1995 [1], all in layers containing up to 10^{10} cm^{-2} extended defects [2]. For lack of bulk GaN, active layers are grown either on sapphire or SiC substrates where the misfit in the basal plane is 16 and 3.5%, respectively. The majority of the defects are dislocations which originate from the interface with the substrate cross the whole epitaxial layer [3–5]. Planar boundaries on the $\{11\bar{2}0\}$ prismatic planes have also been investigated; they have been called double positioning boundaries [6], stacking mismatch boundaries [7] and inversion domain boundaries [5]. It has since been clearly demonstrated that such planar defects have a well defined displacement

† Author for correspondence.

Table 1. Crystallographic data on wurtzite GaN, AlN and the substrates: sapphire and 6H-SiC.

	a (nm)	$\Delta a/a_{SiC}$ (%)	$\Delta a/a_{sap}$ (%)	c (nm)	$\Delta c/c_{SiC}$ (%)	$\Delta c/c_{sap}$ (%)	Thermal expansion coefficients ($\times 10^{-6}$ K)	SG
GaN	0.3189	3.54	16.09	0.5185	2.9	19.7	$\Delta a/a = 5.59$ $\Delta c/c = 3.17$	$P6_3mc$
AlN	0.3112	1.04	13.29	0.4982	1.15	15.06	$\Delta a/a = 4.2$ $\Delta c/c = 5.3$	$P6_3mc$
SiC	0.308			1.512			$\Delta a/a = 4.2$ $\Delta c/c = 4.68$	$P6_3mc$
Sapphire	0.476			1.2991			$\Delta a/a = 7.5$ $\Delta c/c = 8.5$	$R\bar{3}c$

vector and habit plane and therefore can be considered as prismatic stacking faults [8–10]. These faults easily switch from the basal plane in which they always bear the I1 atomic configuration [10].

In this work, we discuss our results on the atomic structure of the extended defects obtained in (Ga, Al)N layers grown by molecular beam epitaxy (MBE) and metallorganic vapour phase epitaxy (MOVPE) on the (0001) surfaces of 6H-SiC or sapphire. Each type was found to exhibit more than one atomic configuration. This is in contrast to the view generally presented in the literature which has tended to demonstrate that the good optical properties of GaN layers were due mainly for example to one specific reconstruction of the atomic cores of the threading dislocations [11, 12]. Moreover analysis of the connection of most of the defects to the substrate/layer interface allowed us to determine some possible mechanisms for their formation.

2. Experiment

The investigated GaN layers were mostly grown on the (0001) sapphire or 6H-SiC surfaces by electron cyclotron resonance (ECR) or NH_3 gas source MBE. The ECR-MBE GaN layers were directly grown at 800 °C at a rate of 40 nm h^{-1}, up to a 2 μm thickness. The NH_3-MBE GaN layers were also deposited at 800 °C but on a low temperature (550 °C) GaN buffer layer (40 nm thickness). A number of layers grown between 1100 and 1150 °C by MOVPE were also investigated: the typical defects that form are intrinsic to the hexagonal structure and do not depend on the growth method; however their nature and density may depend on the growth conditions. The TEM samples were thinned down to 100 μm by mechanical grinding and dimpled down to 10 μm. Electron transparency was obtained by ion milling at 5 kV with a liquid N_2 cold stage at an angle of 15° argon beam incidence. A final step at 3 kV and low angle was used to decrease ion-beam damage. HREM experiments were carried out along the $[11\bar{2}0]$ and [0001] GaN directions on a Topcon 002B electron microscope operating at 200 kV with a point to point resolution of 0.18 nm (Cs = 0.4 mm). HREM images and CBED patterns were simulated using the electron microscopy software [13].

3. Intrinsic properties of GaN and substrate

For now, the growth of active GaN layers is carried out by hetero-epitaxy on a variety of substrates among which sapphire and SiC dominate. Most of the growth has been carried

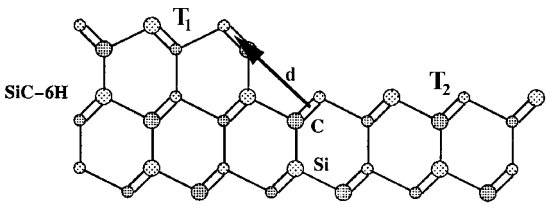

Figure 1. A step model on the (0001) 6H-SIC surface; the associated displacement vector is shown.

Table 2. The four values of the residual translation T_R due to steps h between oxygen terraces at the (0001) surface of sapphire.

Steps	$h/c_{Al_2O_3}$ unit	T_R/c_{GaN} unit	T_R (nm)
A–A or B–B	nc (n: integer)	0	0
A–B	1/6, 5/6, 7/6, 11/6	∼1/12	∼0.0432
A–A or B–B	1/3, 2/3	∼1/6	∼0.0863
A–B	1/2, 3/2	∼1/4	∼0.1295

out on the (0001) surfaces where one has to consider the misfits in the basal plane and the shifts along the $\boldsymbol{c}$ axis which can be introduced at steps (table 1). Along the $\boldsymbol{c}$ axis, this misfit is quite small in the case of 6H-SiC, whereas it is close to 20% on sapphire. Moreover, the stacking sequences of sapphire and GaN are rather different. In the GaN wurtzite system, one has a stacking of two interpenetrating hcp lattices and the 6H packing of SiC is slightly more complex: the stacking is ABC, instead of AB in the case of hcp.

Steps on the (0001) 6H-SiC surface connect terraces by a displacement vector which is either zero, or equal to one of the three stacking fault vectors of the hexagonal lattice (figure 1). When this vector has a component along [0001], an equivalent translation will exist between islands grown on the adjacent terraces.

For growth on (0001) sapphire, the situation is more complex. In sapphire, the oxygen is located at $(x, y, z) = (0.306, 0, 0.25)$, and if this position is approximated to $(x, y, z) \approx (1/3, 0, 1/4)$, the anion framework forms an hcp lattice. The Al^{3+} occupy 2/3 of the octahedral sites but are located at $(x, y, z) = (0, 0, 0.352)$ instead of $(0, 0, 1/3)$, thus the cations are shifted by ± 0.025 nm along the $\boldsymbol{c}$ axis from the ideal octahedral sites. The oxygen ion is larger than the aluminium ion ($r^-/r^+ \approx 3$), therefore the study of the steps on the substrate can be limited to the steps in the oxygen framework, leading to step heights which are multiples of $c/6$ ($d_{(0006)} \approx 0.216$ nm). The (0001) Al_2O_3 surfaces are oxygen terminated [14] and present steps along $\{11\bar{2}0\}$ and $\{10\bar{1}0\}$ planes [15]. A step separating two 'A' surfaces will be denoted for instance (A–A, $c/3$). Steps of height $c/6$, $c/2$ or $5c/6$ separate two surfaces related by a glide symmetry operator; they are energetically degenerate: such steps are called demi-steps [16]; they will be denoted for example (A–B, $c/6$). A simple geometrical analysis shows that even on a flat surface, there are eight possibilities for the growth of a GaN layer. They are either related by displacement vectors and/or an inversion operation [17]. Using $5\boldsymbol{c}$ GaN–$2\boldsymbol{c}$ sapphire, we were able to identify four types of step which lead to a residual translation upon growth on adjacent terraces (table 2).

4. The threading dislocations

These defects originate at the interface between the epitaxial layer and the substrate. Although a large number of them stay in the first tens of nanometres, more than 10^9 cm^{-2} of them reach

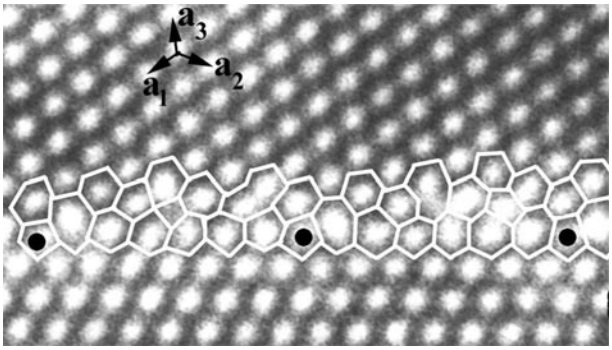

Figure 2. An asymmetric 7 grain boundary in which the three atomic configurations of 4, 5/7, 8 atom cycles for the edge type threading dislocation coexist.

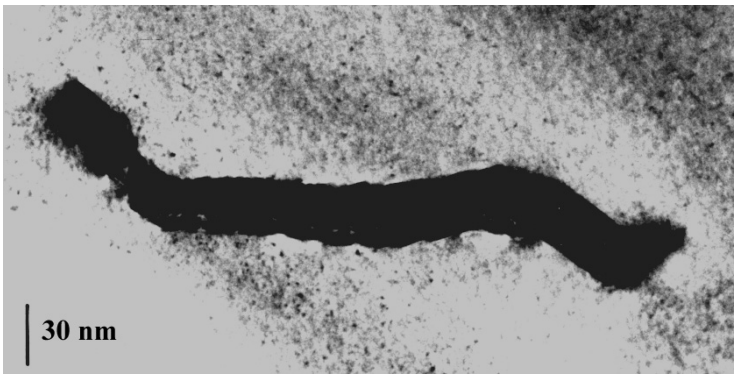

Figure 3. A plane view BF micrograph showing a $\{11\bar{2}0\}$ stacking fault bounded by partial dislocations taken along the [0001] zone axis.

the layer surface in conventional MBE or MOVPE growth. Their line is roughly parallel to the $\boldsymbol{c}$ growth axis and the large majority are of edge type. It has been shown that $\boldsymbol{c}$ and $\boldsymbol{a}+\boldsymbol{c}$ type dislocations tend to bend and annihilate; the density of those that reach the layer surface is only a few per cent of that near the interface [18]. Observations carried out in MOVPE layers [11] and calculations have shown that the low optical activity of the edge threading dislocations may be explained by the formation of dimer bonds inside an eight atom ring core [12]. However, our HREM observations suggest that this may not be the case, at least in MBE grown GaN layers. In addition to the above atomic configuration, we have noticed typical contrast which is not explained by an eight atom core, and from our observations, this configuration has more or less an equal frequency with the eight atom ring core in good layers. Image simulations show that this core is compatible with a 5/7 atom ring configuration [19]. One additional configuration has even been identified in large angle grain boundaries [20], in which three configurations coexist (figure 2).

5. Stacking faults

Apart from the conventional basal stacking faults of the hexagonal system I1, I2, E, a number of workers have identified planar defects that can exist inside the $(11\bar{2}0)$ and $(10\bar{1}0)$ lattice planes.

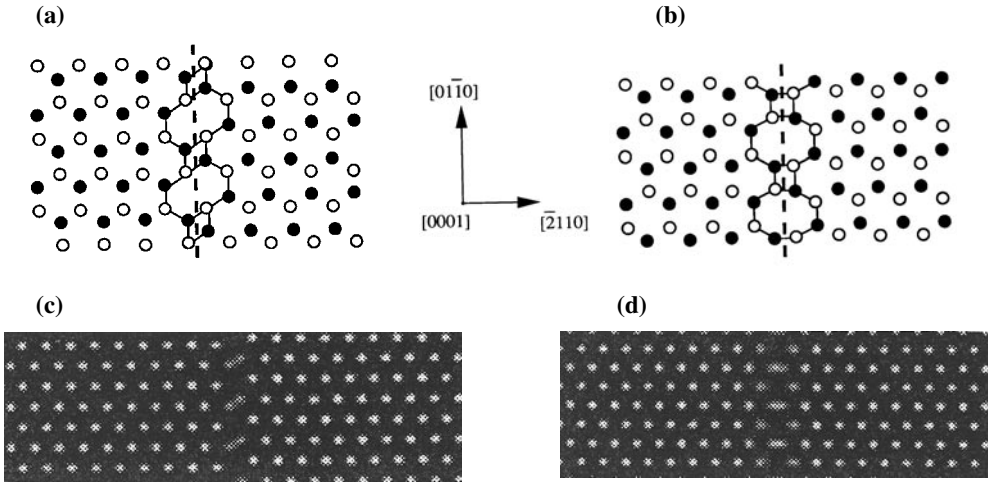

Figure 4. The two models and simulated images for the {11$\bar{2}$0} stacking fault: (a) Blank model, (c) simulated image of Blank model (6 nm thickness, 24 nm defocus), (b) Drum model, (d) simulated image of Drum model.

These defects were first reported in epitaxial ultrathin (10 nm) layers from HREM observations carried out in AlN layers, along the [11$\bar{2}$0] zone axis. As the habit plane could not be determined, the planar boundary was then called a DPB [6]. A subsequent report, which concentrated on the analysis of the stacking difference between SiC and GaN, named these defects stacking mismatch boundaries [7]. The next observations in GaN carried out along [0001], the habit plane was determined and it was demonstrated that these defects lay inside the (11$\bar{2}$0) planes, had a well defined translation displacement vector and folded very easily into and from the basal plane. Inside the basal planes, they always transform into I1. Moreover, they can either form closed domains or be terminated by partial dislocations (figure 3). Similar defects were studied by conventional TEM and their displacement vectors were determined as $1/6[20\bar{2}3]$ [21] and $1/2[10\bar{1}1]$ [22], although no connection was made between them and the stacking faults of the HCP system. The geometrical models of the two defects are shown in figure 4 with the corresponding simulated images along the [0001] zone axis.

Along the [11$\bar{2}$0] zone axis, such defects are projected with an angle of 30°, and, as has been shown elsewhere [10], the projection area exhibits characteristic features for each model. The Drum model shows pseudo-hexagonal contrast whereas the Blank model exhibits high contrast for one lattice row in two. Investigated GaN layers mostly exhibit stacking faults corresponding to the Drum model which systematically originate from the I1 $= 1/6[20\bar{2}3]$ type of steps at the substrate surface (figure 5(a)).

Inside the AlN buffer layers, it was possible to identify the two atomic configurations which were connected by a basal I1 stacking fault (figure 5(b)). Therefore, as this boundary can be limited by partial dislocations and that it continuously folds in the {0001} and {11$\bar{2}$0} planes as for example in B and C in figure 5(b), one can use the name stacking fault to designate it.

6. Inversion domain boundaries

Inversion domains are symmetry variants in the wurtzite structure due to the polar character of the spatial group ($P6_3mc$); in other words the two tetrahedral sites of the anion sublattice

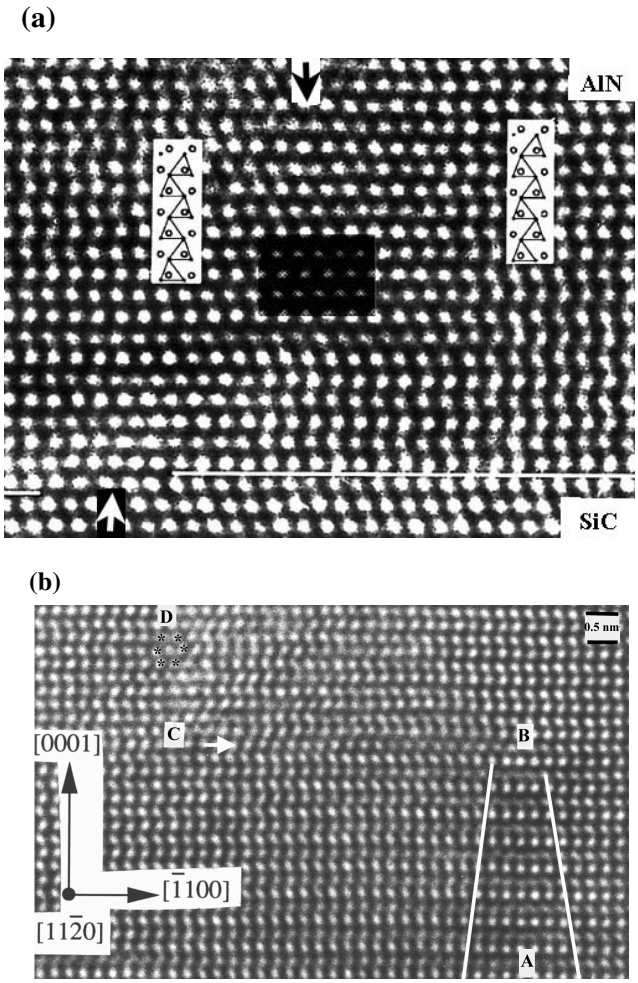

Figure 5. HREM images of the {11$\bar{2}$0} stacking fault: (a) connection of the fault to an interface step; (b) coexistence of the Drum (C–D) and Blank (A–B) configurations connected by a basal I1 stacking fault (B–C).

cannot be simultaneously occupied by the cations. In recent work, their formation was found to depend on the growth parameters such as substrates used [9], buffer layer thickness and growth temperature [18]. In epitaxial GaN, it is now admitted that they tend to develop in the N polar matrix in which they grow at a higher rate and usually reach the layer surface in the centre of pyramidal features [23]. In Ga polar layers, the inversion domains are confined to the interfacial area [24]. The domains that reach the epitaxial layer surface are limited by {10$\bar{1}$0} facets [25]. A number of results have been published on the atomic structure of their boundaries (IDB); *ab initio* calculations have shown that, due to the ionic character of the compound, the IDB can have low energy if it only contains Ga–N bonds [26]. In our work, no inversion domains have been observed in layers grown on SiC; this is agreement with other authors who have found that there is a strong substrate effect underlying their formation [27]. In GaN layers grown on (0001) sapphire, two types of sample containing inversion domains were identified by their surface morphologies [28]. Some have flat surfaces, whereas others

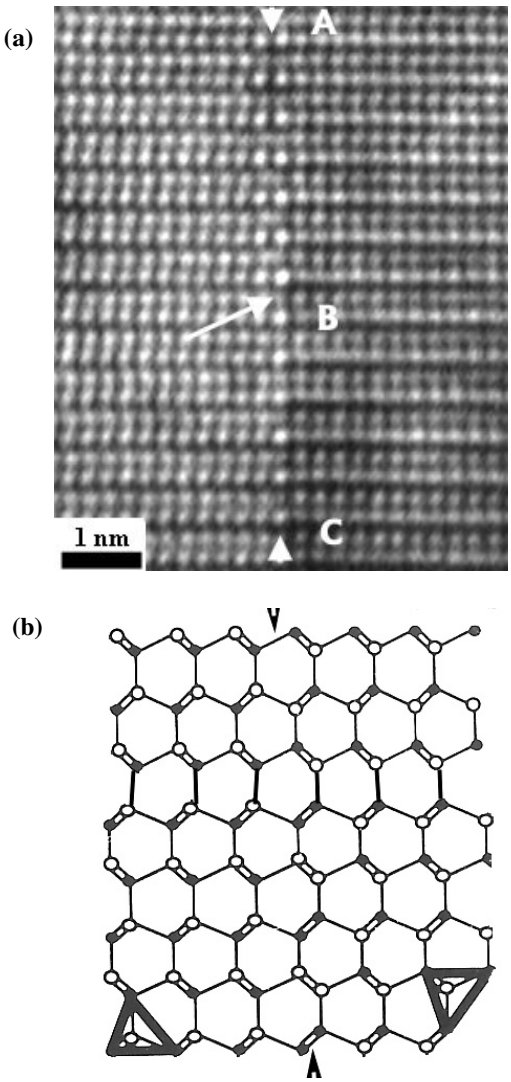

Figure 6. Switching of an inversion domain boundary from shuffle to glide position: (a) HREM image; (b) corresponding Holt model.

exhibit small pyramids with a surface roughness of about 100–200 nm. In this case, inversion domains up to 50 nm in width were located in the centres of the pyramids. In the former, a high density of smaller inversion domains could be found inside the layer, less than 20 nm in size.

A detailed investigation of the atomic structure of the boundary planes was carried out, using HREM and extensive image simulations; it was found that the two types of sample were characterized by inversion domains with different boundaries. The image simulation work took into account various models including the Austerman type [29]. In the flat surface layers the IDBs could be described by the model proposed by Holt [30], in which the Ga and N atoms are only interchanged across the boundary [31]. For the largest domains, the boundary could be described by the 'V' configuration in which one has an additional $\boldsymbol{c}/2$ translation of one

Table 3. Steps expressed in terms of the IDB operation: α is the remaining shift along the $\boldsymbol{c}$ axis, after the formation of an IDB, WB is an Austerman type of IDB.

Step notation in $c_{Al_2O_3}$ unit	$W_{ce} = T_{step}$	$W'_{ce} = W_{ce} \pm m$	$W'_{ce} = W_{IDB} + \alpha[0001]$
(A–B, $c/6$)	$R_E - 1/12[0001]$	$R_E - 1/12[0001] + m$	$W_{Holt} + 1/24[0001]$
(A–A, $c/3$)	$-1/6[0001]$	$-1/6[0001] + m$	$W_V - 1/24[0001]$
(A–B, $c/2$)	$1/4[0001]$	$1/4[0001] + m$	W_B
(A–A, $2c/3$)	$R_E + 1/6[0001]$	$R_E + 1/6[0001] - m$	$-W_{Holt} + 1/24[0001]$
(A–B, $5c/6$)	$1/12[0001]$	$1/12[0001] - m$	$-W_V - 1/24[0001]$
(A–B, $c + c/6$)	$-1/12[0001]$	$-1/12[0001] + m$	$W_V + 1/24[0001]$
(A–A, $c + c/3$)	$R_E - 1/6[0001]$	$R_E - 1/6[0001] + m$	$W_{Holt} - 1/24[0001]$
(A–B, $c + c/2$)	$-1/4[0001]$	$-1/4[0001] - m$	W_B
(A–A, $c + 2c/3$)	$1/6[0001]$	$1/6[0001] - m$	$-W_V + 1/24[0001]$
(A–B, $c + 5c/6$)	$R_E + 1/12[0001]$	$R_E + 1/12[0001] - m$	$-W_{Holt} - 1/24[0001]$

crystal from the Holt model in order to avoid the formation of Ga–Ga or N–N bonds. This model has been independently observed by other authors and called IDB* [26]. During this work, we did not notice any switching from one configuration to the other inside the same type of sample. In contrast, as shown in figure 6(a), it is possible, for the two configurations, that the boundary plane be located in the glide or shuffle positions, thus breaking one or two bonds per atom (figure 6(b)).

7. Formation mechanisms

Although no clear connection has yet been shown between the interface to the substrate and the threading dislocations, it has been suggested that they are due to growth errors which give rise to small rotations (0.5–1.5°) between adjacent islands [32]. This mechanism is now generally admitted and has been called the mosaic growth mode; it agrees quite well with the microstructure of the GaN layers in which not only small angle boundaries are exhibited but where large angle grain boundaries may be found [20]. A recent detailed *in situ* analysis has shown that these dislocations form during the early stages of growth, and when the pseudo-2D mode is attained, they do not influence the growth front [33]. It seems that they appear upon the coalescence of the initial 3D islands, which may already be relaxed by the formation of interfacial misfit dislocation network. It would then be of interest to understand how the two dislocation systems interact as this determines the transmission of these defects inside the epitaxial layer.

The $\{11\bar{2}0\}$ planar defects which occur in the epitaxial layers of GaN are identical to those identified earlier by Blank *et al* in 1964 [21] in AlN which exhibited a $1/6[20\bar{2}3]$ displacement vector. They were analysed as growth defects which could not have been generated under deformation. In GaN layers grown on 6H-SiC, they have been systematically been related to surface steps with displacement vector component parallel to the $\boldsymbol{c}$ growth axis, especially I1 type of step which are quite frequent on the SiC surface [9].

On sapphire such displacement vectors can even relate islands which nucleate on a flat surface due to the many possible stacking possibilities which face the first Ga and N atoms impinging on that surface. The switching from the octahedral occupation to the tetrahedral site of GaN allows for eight geometrical configurations related by either translation operations or the inversion: four of them are shown in figure 7; a detailed analysis can be found in [17]. At steps, there is mainly a residual translation along the growth axis and it cannot be reduced

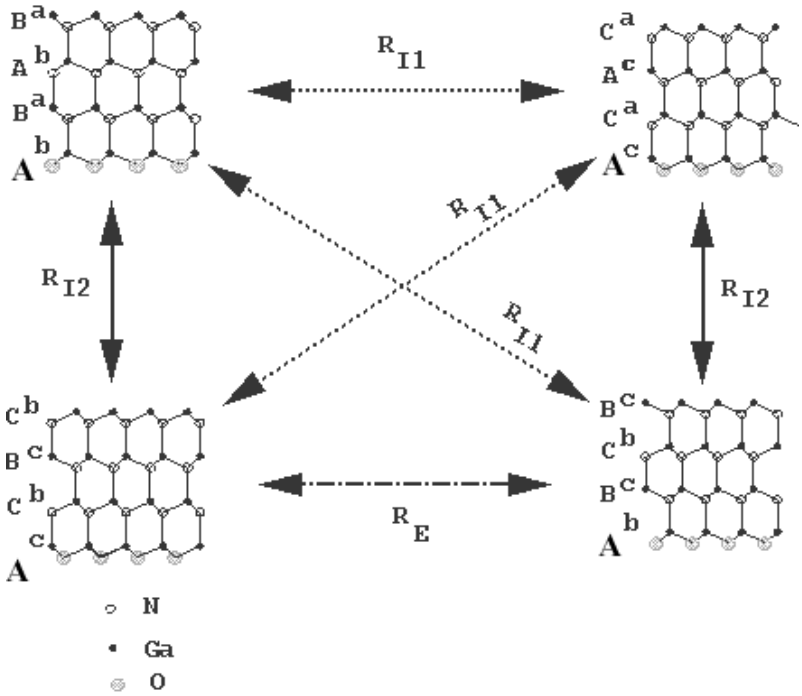

Figure 7. Four of the eight possibilities for GaN to deposit on the (0001) sapphire surface; their mutual connection by displacement vectors.

by any of the hcp stacking faults displacement vectors. However by introducing an inversion between two adjacent crystallites, this translation is minimized by the formation of IDBs as shown in column 4 of table 3.

In this analysis, it can be seen that the two observed configurations of IDBs are equally efficient and their occurrence may possibly be explained by the surface structure of the substrate [34]. The Holt model IDBs appear to form on small surface steps, whereas the V configuration will take place on slightly larger ones. When large steps are present, as made on the surface by a large misorientation, both configurations are found to disappear [35].

8. Conclusion

This structural analysis has shown that each extended defect exhibits more than one atomic configuration in GaN. The threading dislocations have three different configurations, among which the 5/7 atom rings exhibit wrong bonds. The four atom ring core has four in plane bonds, which implies that it is highly strained. Among these configurations the eight atom ring core has been investigated in detail for its possible electrical activity. The prismatic stacking fault is directly related to the I1 stacking fault but bears two atomic configurations; until now no data about its electrical activity have been reported. Additionally one of the two configurations pointed out for the inversion domain boundaries contains also wrong bonds. Therefore, it is clear that more work is needed in order to understand the connection between the atomic structure of such defects and the properties of the active layers.

Acknowledgments

This work is supported by the EU under contract HPRN-CT-1999-00040.

References

[1] Nakamura S, Senoh M, Nagahama S, Iwasa N, Yamada T, Mitsushita T, Kiyoku H and Sugimoto Y 1996 *Japan. J. Appl. Phys.* **35** L74
[2] Ponce F A, Major S J, Plano W E and Welch D F 1994 *Appl. Phys. Lett.* **65** 2302
[3] Lester S D, Ponce F A, Crawford M G and Steigewald D A 1995 *Appl. Phys. Lett.* **66** 1249
[4] Vermaut P, Ruterana P, Nouet G, Salvador A, Botchkarev A and Morkoç H 1995 *(Inst. Phys. Conf. Ser. 146)* (Bristol: Institute of Physics) p 289
[5] Rouvière J L, Arlery M, Niebuhr R and Bachem K 1995 *(Inst. Phys. Conf. Ser. 146)* (Bristol: Institute of Physics) p 285
[6] Tanaka S, Kern R S and Davis R F 1995 *Appl. Phys. Lett.* **66** 37
[7] Sverdlov B N, Martin G A, Morkoç H and Smith D J 1995 *Appl. Phys. Lett.* **67** 2063
[8] Vermaut P, Ruterana P, Nouet G and Morkoç H 1997 *Phil. Mag.* A **75** 239
[9] Vermaut P, Ruterana P and Nouet G 1997 *Phil. Mag.* A **76** 1215
[10] Vermaut P, Nouet G and Ruterana P 1999 *Appl. Phys. Lett.* **74** 694
[11] Xin Y, Pennycook S J, Browing N D, Nellist P D, Sivanathan S, Beaumont B, Faurie J P and Gibart P 1998 *Mater. Res. Soc. Symp. Proc.* vol 482 (Pittsburgh, PA: Materials Research Society) p 781
[12] Elsner J, Jones R, Sitch P K, Porezag V D, Elstner M, Fraunheim T, Heggie M I, Oberg S and Briddon P R 1997 *Appl. Phys. Lett.* **79** 3672
[13] Stadelmann P 1987 *Ultramicroscopy* **21** 131
[14] Kung P, Sun C J, Saxler A, Ohsato H and Razeghi M 1994 *J. Appl. Phys.* **75** 4515
[15] Susnitzky D W and Carter C B 1986 *J. Am. Ceram. Soc.* **69** C-217
[16] Pond R C, Gowers J P and Joyce B A 1985 *Surf. Sci.* **152** 1191
[17] Ruterana P, Potin V, Barbaray B and Nouet G 2000 *Phil. Mag.* A **80** 937
[18] Rouvière J L, Arlery M and Bourret A 1997 *(Inst. Phys. Conf. Ser. 157)* (Bristol: Institute of Physics) p 173
[19] Ruterana P, Potin V and Nouet G 1998 *Mater. Res. Soc. Symp. Proc.* vol 482 (Pittsburgh, PA: Materials Research Society) p 72
[20] Potin V, Ruterana P, Nouet G, Pond R C and Morkoç H 2000 *Phys. Rev.* B **61** 5587
[21] Blank H, Delavignette P, Gevers R and Amelinckx S 1964 *Phys. Status Solidi* **7** 747
[22] Drum C M 1965 *Phil. Mag.* A **11** 313
[23] Romano L T and Myers T H 1997 *Appl. Phys. Lett.* **71** 3486
[24] Rouvière J L, Arlery M, Niebuhr R, Bachem K H and Briot O 1996 *MRS Int. J. N.S.R.* **1** paper 33
[25] Potin V, Nouet G and Ruterana P 1999 *Phil. Mag.* **79** 2899
[26] Northrup J E, Neugebauer J and Romano L T 1996 *Phys. Rev. Lett.* **77** 103
[27] Ponce F A, Bour D P, Götz W, Johnson N M, Helava H I, Grezgory I, Jun J and Porowski S 1996 *Appl. Phys. Lett.* **68** 917
[28] Potin V, Nouet G and Ruterana P 1999 *Appl. Phys. Lett.* **74** 947
[29] Austerman S B and Gehman W G 1966 *J. Mater. Sci.* **1** 249
[30] Holt D B 1969 *J. Phys. Chem. Solids* **30** 1297
[31] Potin V, Ruterana P and Nouet G 1997 *J. Appl. Phys.* **82** 1276
[32] Ning X J, Chien F R, Pirouz P, Yang J W and Khan A M 1996 *J. Mater. Res.* **11** 580
[33] Vézian S, Massies J, Semond F, Grandjean N and Vennéguès P 2000 *Phys. Rev.* B **61** 7618
[34] Barbaray B, Ruterana P and Nouet G 1999 *Diamond Relat. Compounds* **8** 314
[35] Barbaray B, Ruterana P and Nouet G, di Forte Poisson M A, Huet F and Torjman M 1999 *Microscopy of Semiconducting Materials (Inst. Phys. Conf. Ser. 164)* (Bristol: Institute of Physics) p 385